CCFE-PR(15)82

S. C. Guo, X. Y. Xu, Y. Q. Liu and Z. R. Wang

Fishbone-like external kink instability and its co-existence and coupling with the resistive wall mode

Fishbone-like external kink instability and its co-existence and coupling with the resistive wall mode

S. C. Guo[1], X. Y. Xu[1], Y. Q. Liu [2] and Z. R. Wang [3]

[1]Consorzio RFX, Corso Stati Unit 4, 35127 Padova, Italy
[2]CCFE, Culham Science Centre, Oxon OX14 3DB, UK
[3]Princeton Plasma Physics Laboratory, Princeton, NJ 08543, USA

Fishbone-like external kink instability and its co-existence and coupling with the resistive wall mode

S. C. Guo[1], X. Y. Xu[1], Y. Q. Liu [2], Z. R. Wang [3]

[1]Consorzio RFX, Corso Stati Unit 4, 35127 Padova, Italy

[2] CCFE, Culham Science Centre, Oxon OX14 3DB, UK

[3] Princeton Plasma Physics Laboratory, Princeton, NJ 08543, USA

ABSTRACT

An unstable fishbone-like non-resonant external kink mode (FLEM) is numerically found to be driven by the precessional drift motion of trapped energetic particles (EPs) in both RFP and Tokamak plasmas. The FLEM originates from a stable external ideal kink mode, which is stabilized by a close-fitting ideal conducting wall. In the presence of a sufficiently large fraction of EPs in the plasma, and with the satisfaction of the resonance condition $n\omega_d \approx \omega_r - n\Omega$ (ω_d is the precession frequency of trapped EPs, ω_r the kink mode frequency and Ω the plasma toroidal rotation frequency), the FLEM instability occurs. The frequency of the FLEM, therefore, varies with the plasma flow speed, and is usually much higher than that of the typical resistive wall mode (RWM). In general, the growth rate of FLEM does not depend on the wall resistivity. However, the wall position can significantly affect the mode's property. The drift kinetic effects from thermal particles (mainly due to the transit resonance of passing particles) play a stabilizing role on FLEMs. In the presence of EPs, the FLEM and the RWM can co-exist or even couple to each other, depending on the plasma parameters. The FLEM instabilities in RFP and Tokamak have rather similar physics nature, although certain sub-dominant characters appear differently in the two configurations

1. Introduction

The energetic particle physics is an important issue to be studied in order to understand the behavior of the burning plasmas which represents the primary scientific challenge faced by ITER and fusion research in general. E.g., self-heating in Fusion reactor is provided by the alphas generated at 3.5MeV by the D–T fusion reactions. In addition, other energetic ions, generated by neutral beam injection (NBI) and ion cyclotron resonant heating (ICRH), are expected to play major role in achieving optimal burning plasma scenarios with external heating and/or current drive. On the other hand, the Energetic Particles (EPs) may interact with the bulk plasma waves and instabilities, which possibly lead to destabilize/stabilize the existing turbulence in the bulk plasma, even to excite a new type of instabilities, which may result to redistribution and losses of EPs.

It is well-known that future advanced tokamak devices (AT) need to steadily operate in a rather high-β region ($\beta = 2\mu_0 P/B^2$, the ratio of the plasma pressure to the magnetic field pressure). However, the achievable maximum β is often limited by macroscopic MHD instabilities such as the external kink mode[1], which causes a global distortion of the plasma that often results in a major disruption. Although, under a limit value of β (so-call ideal wall beta limit) the external kink mode can be completely stabilized by a perfectly conducting wall located close enough to the plasma surface, it could convert to other unstable branches under certain circumstances. The most well-known destabilizing mechanism is the replacement of the ideal wall with a realistically existing resistive wall in the fusion experimental devices, which allows the magnetic perturbation of the kink penetrates through the wall and leads to the Resistive Wall Mode (RWM) instability[1,2]. In this work, instead, we study another destabilizing mechanism: the precession drift motion of the trapped energetic ions can induce the Fishbone-like External kink Mode (FLEM) instability even under an ideal wall condition.

The original experimentally observed Fish-bone instability[3] has been well studied theoretically around years 80s[4,5]. It was reported that the trapped energetic particles provide an additional destabilizing mechanics, producing a new unstable branch to the internal kink mode dispersion relation.

In the recent Tokamak experiments, a fishbone-like bursting modes are newly observed and studied when NBI were applied[6-9]. Theoretical studies[10,11] also found a new branch in the presence of trapped EPs by the analytical solution of the RWM dispersion relation. Furthermore, an unexpected high frequency (comparable to geodesic acoustic mode and beta induced Alfven eigenmode) fishbone has also been observed in JET experiments, and theoretic interpretation is provided by a new suitable dispersion relation[12,13 14]. In RFPs, only recently NBI is applied on the Madison Symmetric Torus (MST) and the energetic particle induced MHD fluctuations are observed[15-17].

All those works provided helpful investigations on the physics of energetic particle interacting with the global MHD mode. Certainly still a wide area on this problem remains to be further studied.

In this work we numerically study the energetic ions interacting with MHD external kink mode in both RFP and tokamak plasmas and make comparison between the two configurations. This study would be much relevant to the current and future experiments with the presence of EPs. Toroidal stability code MARS-K is adopted in the study, where the drift kinetic theory for both Energetic ions and bulk thermal particles are self-consistently involved. It is found that the Fishbone like-external kink mode instability can be driven by the precessional drift motion of the trapped energetic ions in both tokamak and RFPs even in the plasmas surrounded by an ideal wall. The various physical natures of the FLEM are further clarified by the numerical analyses, and its relation with the RWM (co-existence/coupling) is also investigated. The FLEM satisfies the external kink dispersion relation, in which the kinetic effects of the hot ions are considered. The kinetic contribution by trapped hot ions is a unique destabilizing (driving) mechanism for FLEM instability. While for RWM, the trapped hot ions alone can play only a stabilizing (damping) role through their kinetic contribution to the energy component in the dispersion relation.

The paper is organized as the follows: Section 2 describes the kinetic-MHD hybrid theoretical model and the formulation, as well as the equilibrium model of EPs used in this work. Section 3 is devoted to the investigation of the FLEM in RFP configuration, the discussion of the physics mechanism of the FLEM instability and related nature of the modes. The possibility of co-existence/coupling with RWM is also presented. Section 4 presents the study of FLEM in tokamak plasmas (circular cross section with a similar geometry as RFP), and the compares the various natures of FLEM with what shown for RFP plasmas. Physics understanding is also provided by the numerical analysis. The summary and a brief discussion are presented in Section 5.

2. Models and formulations

2.1 Toroidal self-consistent MHD-kinetic hybrid model

The MARS-K code numerically solves the linearized, single fluid MHD equations with self-consistent inclusion of drift kinetic resonances in toroidal geometry [18]. For a given curvilinear flux coordinate system (s, χ, φ), and by assuming that all the perturbations have the form $A(s, \chi, \varphi, t) = A(s, \chi)\, e^{-i\omega t - in\varphi}$, the MHD equations are written in the Eulerian frame in the code

$$-i\left(\omega - n\Omega\right)\boldsymbol{\xi} = \mathbf{v} + \left(\boldsymbol{\xi}\cdot\nabla\Omega\right)R^2\nabla\phi \tag{1}$$

$$-i\rho\left(\omega - n\Omega\right)\mathbf{v} = -\nabla\cdot\mathbf{p} + \nabla\times\mathbf{Q}\times\mathbf{B} + \nabla\times\mathbf{B}\times\mathbf{Q} - \rho\left[2\Omega\hat{\mathbf{Z}}\times\mathbf{v} + \left(\mathbf{v}\cdot\nabla\Omega\right)R^2\nabla\phi\right] \tag{2}$$

$$-i(\omega - n\Omega)\mathbf{Q} = \nabla\times(\mathbf{v}\times\mathbf{B}) + (\mathbf{Q}\cdot\nabla\Omega)R^2\nabla\phi \quad (3)$$

$$\mathbf{p} = p_{\parallel}\mathbf{bb} + p_{\perp}(\mathbf{I} - \mathbf{bb}) \quad (4)$$

$$\text{And } p_{\parallel} = \sum_j \int M_j v_{\parallel}^2 f_j^1 d\Gamma,\ p_{\perp} = \sum_j \int \frac{1}{2} M_j v_{\perp}^2 f_j^1 d\Gamma \quad (5)$$

where s is the normalized radial coordinate labeling the equilibrium flux surface. χ is a generalized poloidal angle. $\omega = \omega_r + i\gamma$ is the complex eigenvalue of the mode (γ being the mode growth rate, ω_r the mode rotation frequency in the laboratory frame). The mode frequency is corrected by a Doppler shift $in\Omega$, with n being the toroidal mode number, Ω the plasma rotation frequency in the torodial direction ϕ. $\boldsymbol{\xi}$, **v**, **Q**, **j**, **p** represent the perturbed quantities: the plasma displacement, the perturbed velocity, magnetic field, current and kinetic pressure tensor, respectively. ρ is the unperturbed plasma density. **B** is the equilibrium magnetic field. R is the plasma major radius. $\hat{\mathbf{Z}}$ is the unit vector in the vertical direction. A conventional unit system is assumed with the vacuum permeability μ_o=1; and the subsonic plasma flow is assumed.

The perturbed kinetic pressure tensor **p** includes both parallel (to the equilibrium magnetic field), $p_{||}$, and perpendicular, $p_{\perp}$, components. Each component involves both adiabatic (superscript "a") and non-adiabatic (superscript "na") parts: $p_{||}=p_{||}^{a}+p_{||}^{na}$, $p_{\perp}= p_{\perp}^{a}+ p_{\perp}^{na}$.

$$p_g^a = \sum_j \int d\Gamma E_g(-\xi_{\perp}\cdot\nabla f_j^o), \quad (6)$$

$$p_g^{na} = \sum_j \int d\Gamma E_g f_j^1 \qquad g = \parallel, \perp, \quad (7)$$

Where $E_{\parallel}=Mv_{||}^2$, and $E_{\perp} = Mv_{\perp}^2$. **I** is the unit tensor, and **b**= **B**/|B|. Γ denotes the velocity space of particles, and j denotes the particle species including thermal ions and electrons as well as energetic ions (j=i,e,a). f^{o}_{j} is the equilibrium distribution function. f_j^l, is the solution of the perturbed drift kinetic equation, which we solve together with the fluid equations[19,20]. Therefore this self-consistent approach provides a drift kinetic closure to the single fluid MHD equations. Besides, a set of vacuum equations for the perturbed magnetic field ***Q***, and the resistive wall equation based on the thin-shell approximation, are solved together with equations (1)–(4) [21].

We assume a Maxwellian equilibrium distribution for the thermal ions and electrons, and adopt a slowing down distribution for the energetic ions (In the next, we use "EPs" referring to the

energetic ions), simulating the energetic alpha particles and /or fast ions produced by the neutral beam injection[22] :

$$f_a^o(\psi,\varepsilon_k)=\begin{cases}\dfrac{c(\psi)}{\varepsilon_k^{3/2}+\varepsilon_c^{3/2}} & 0<\varepsilon_k<\varepsilon_\alpha \\ 0 & \varepsilon_k>\varepsilon_\alpha\end{cases} \qquad \textbf{(8)}$$

Where $\varepsilon_c=(\frac{3\sqrt{\pi}}{4})^{2/3}(\frac{M_a}{M_i})(\frac{M_i}{M_e})^{1/3}T_e$, M_i, M_e and M_a denote the mass of thermal ion, electron and energetic ion respectively; The constant ε_α is the so called birth energy, defined as

$$\varepsilon_\alpha=\begin{cases}3.5Mev & \alpha\text{-particles} \\ \varepsilon_\alpha(s) & \text{beam-driven fast ions}\end{cases} \qquad (9)$$

The c(ψ) is a normalization factor, determined by $N_a=\int f_a^o d\Gamma$. N_b is the Eps' density.

The drift kinetic effects from each spices of particles are self-consistently coupled to MHD equations; the detail description can be found in Ref.[18]. For the thermal particles, the key element in this formulation is the wave-particle resonance operator, expressed as

$$\lambda_{ml}^{\alpha}=\frac{n\left[\omega_{*N}+\left(\varepsilon_k-3/2\right)\omega_{*T}+\Omega\right]-\omega}{n\omega_d+\left[\alpha\left(m+nq\right)+l\right]\omega_b+n\Omega-\omega-i\nu_{eff}} \qquad \textbf{(10)}$$

where $\omega=\omega_r+i\gamma$, ω_d is the bounce-orbit-averaged precession drift frequency. For trapped particles, $\alpha=0$, and ω_b is the bounce frequency. For passing particles, $\alpha=\pm1$, and ω_b represents the transit frequency. Similar to thermal particles, the precessional drift resonance operators for fast ions can be expressed as

$$\lambda^a=\frac{n(\frac{\partial f_a^o}{\partial\psi}/Ze\frac{\partial f_a^o}{\partial\varepsilon})-\omega}{n\omega_{da}+n\Omega-\omega-i\nu_{eff}} \qquad \textbf{(11)}$$

Where ω_{da} is the bounce orbit averaged precession drifts frequency of the fast ions. To start with, we ignored the finite banana orbit effect in the study and consider only the isotropic energetic particle distribution. These two effects can be readily extended to the further studies.

2.2 Quadratic energy term

In order to gain better physical understanding, we compute various components of the quadratic energy form[23,24], for both fluid and drift kinetic energy perturbations, from the self-consistent solution. We define the following energy components of the fluid potential energy δW_F and the kinetic potential energy δW_k.

$$\delta W_F = \delta W_j + \delta W_Q + \delta W_p \tag{12}$$

Where

$$\delta W_j = \frac{1}{2}\int |Q|^2 J ds d\chi d\phi$$

$$\delta W_Q = \frac{1}{2}\int \left[J_{\square}\mathbf{b}\cdot\xi_\perp^* \times \mathbf{Q}_\perp - \frac{Q_{\square}}{B}(\xi_\perp^* \cdot \nabla P) \right] J ds d\chi d\phi$$

$$\delta W_p = \frac{1}{2}\int (\nabla \cdot \mathbf{p}^a)\cdot \xi_\perp^* J ds d\chi d\phi$$

J is the Jacobian of the flux coordinates. The kinetic energy term is obtained as

$$\delta W_K = \frac{1}{2}\int_{V^P} J ds d\chi d\phi \left[p_\perp^{na} \frac{1}{B}\left(Q_{//}^* + \nabla B \cdot \xi_\perp^*\right) + p_{//}^{na} \boldsymbol{\kappa}\cdot\xi_\perp^* \right] \tag{13}$$

Taking into account the eq (7), the kinetic energy component contributed from the thermal ion and electrons can be expressed as [ ]

$$\delta W_k^{e,i} = \frac{\nu\sqrt{\pi}}{2B_0}\sum_{e,i}\int d\Psi P_{e,i}\left\{ \int d\varepsilon_k \varepsilon_k^{5/2} e^{-\varepsilon_k} \sum_\sigma \left[\int d\Lambda \sum_l \lambda_l^\alpha \hat{\tau}_b \left| \left\langle e^{-i(l+\alpha nq)\omega_b t - in\phi} H_L^{e,i} \right\rangle_l \right|^2 \right] \right\}$$

where Ψ is the equilibrium poloidal flux, $P_{e,i}$ denotes the ion and electron equilibrium pressure, $\Lambda = B_0\mu/\varepsilon_k$ (B_0 is the on-axis field strength), $\sigma = sign(v_{\square})$. The integration is taken in both the real and the velocity spaces. The sum is over the poloidal Fourier harmonics m and bounce harmonics l, the passing and trapped particles, as well as the particle species (e, i). For trapped particles, α=0, ν =1/2 and $\hat{\tau}_b$ is the bounce period normalized by a factor $\sqrt{M/2\varepsilon_k}$; for passing particles, α= σ, ν =1 and $\hat{\tau}_b$ represents the normalized transit period. < > denotes the time average over the bounce/transit period.

The contribution from the trapped energetic particles (ions) is written

$$\delta W_k^\alpha = \frac{1}{2}\int dx^3 \int d\Gamma \varepsilon_k \left(-\frac{\partial f_a^o}{\partial \varepsilon_k}\right)\lambda^a \left| \left\langle e^{in\tilde{\phi}(t)} H_L^a(t) \right\rangle \right|^2 \tag{14?}$$

H_L^j is the perturbed particle Lagrangian of the j species[20].

$$H_L^j(s,\chi,\Lambda) = 2\left(1-\frac{\Lambda}{h}\right)\boldsymbol{\xi}_\perp\cdot\boldsymbol{\kappa} + \frac{\Lambda}{B_0}\left(Q_\parallel + \boldsymbol{\xi}_\perp\cdot\nabla B\right) \tag{15}$$

where $h = B_0 / B$. The total kinetic energy component is the combination of the contribution from the all particle species. $\delta W_k = \sum_j \delta W_k^j$.

In the energy calculations, we neglect the centrifugal and the Coriolis force terms in the RHS of Eq. (2), assuming a slow (subsonic) equilibrium flow. The vacuum energy, $\delta W_{v\infty}$ and δW_{vb}, without wall and with an ideal wall at the minor radius b, respectively, are written as

$$\delta W_{v\infty} = \frac{1}{2}\int_{V^\infty} |\mathbf{Q}|^2 \, J ds d\chi d\phi = -\frac{1}{2}\int_{S^p} b_1^n \hat{V}_1^{*\infty} J_s d\chi d\phi \tag{16}$$

$$\delta W_{vb} = \frac{1}{2}\int_{V^b} |\mathbf{Q}|^2 \, J ds d\chi d\phi = -\frac{1}{2}\int_{S^p} b_1^n \hat{V}_1^{*b} J_s d\chi d\phi \tag{17}$$

where b_1^n is the normal magnetic field perturbation $V_1^{*\infty,b}$ is the complex conjugate of the perturbed magnetic scalar potential, which is determined by the ideal wall position and b^n_1 at the plasma surface [24]. In the above calculations, we have considered cases with vanishing perturbed surface currents, and with vanishing equilibrium pressure at the plasma edge, i.e. $P(a)$=0.

2.3 The equilibrium profiles of the energetic particles.

In the following study, the density fraction and pressure fraction of EPs' with respect to the bulk thermal particles are denoted by N*=N_a/N_e, and by P*= P_a/P_{th} respectively , where the subscripts "a" ,"e" and "th" denote the species of EPs ($P_a = \frac{2}{3}\int f^o \varepsilon_k d\Gamma \propto N_a \varepsilon_\alpha$), electrons and the bulk thermal particles (ions plus electrons). The total plasma pressure is $P_{total}= P_{th} + P_a$. Both N* and P* are the functions of s, which is the coordinate linked to the poloidal magnetic field fluxes.

Consequently the beta fraction of energetic particles is denoted by β*, $\beta^*=\beta_a/\beta_{th}$. For RFPs, the poloidal beta value β_p is commonly in use, while in tokamaks the total beta value β is usually used in the plasma description. By seeking convenience for the numerical analysis, we consider two types of the P*(s) profiles (normalized by B_o^2/μ_o): (1) P*(s)= β_o^* ,which is a constant along the minor radius, thus $\beta^*= \beta_o^*$.(2) $P^*= \beta_o^*(1-s^2)^8$, in which, obviously, the value of β* appears much smaller than β_o^*. As examples, in Fig.1, corresponding to type (1) and $\beta^*=\beta_o^*$= 0.3, the equilibrium pressure (a) and density profiles (b) of the hot ions, bulk thermal particles, and total

particles are plotted separately. Fig.2 shows the pressure and density profiles of type (2), where β_o*=1.0 and β*=0.176.

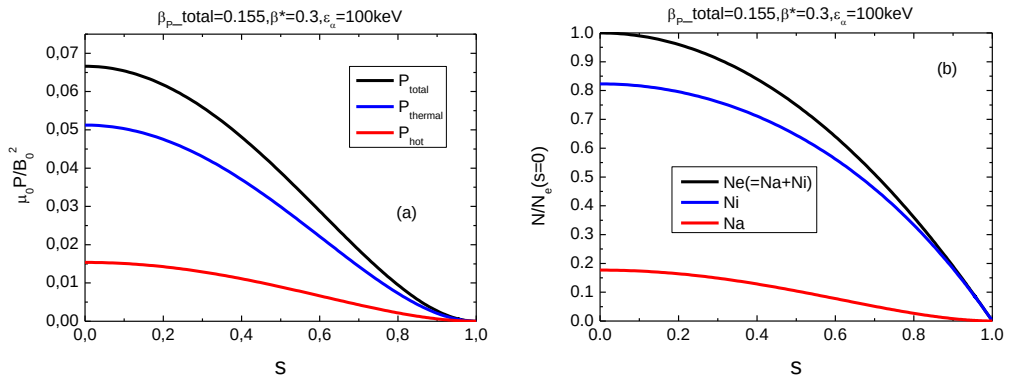

Fig. 1 The equilibrium profiles corresponding to case P=constant are plotted. (a)The pressure profiles (normalized by B_o^2/μ_o) for the hot ions, bulk thermal particles and total particles; (b) density profiles (normalized by Ne(s=0) at the magnetic axis) for the thermal ions(N_i) and electrons(N_e), as well as the energetic ions(N_a). The equilibrium parameters are Pa/Pth=0.3(β*=β_o*=0.3)., β_p=0.155, and ε_α=100kev.*

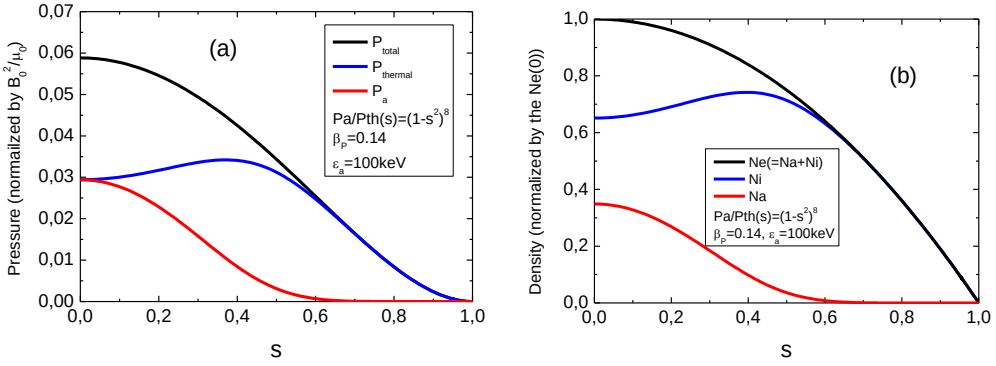

Fig.2. The equilibrium profiles corresponding to $P^*(s)=\beta_0^*(1-s^2)^8$ are plotted. (a) The pressure profiles (normalized by B_o^2/μ_o) of the hot ions, the bulk thermal particles and the total particles; and (b) the density profiles (normalized by the $N_e(0)$ at the magnetic axis) for the thermal ions (N_i) and the electrons(N_e) as well as the energetic ions (N_a). β_p=0.14 and ε_α=100kev, β=0.176, (β_o*=1.0).*

The profile of Fig.2 will be used in the most following computations without specific statement. The profile of β*=β_o^*=constant is used in a few numerical analyses for seeking a simplicity, which will be stated at the figure captions. The difference of these two profiles does not cause a qualitative change on the nature of the FLEM instabilities.

3. 3. FLEM in RFP plasmas

4. In this paper we firstly discuss the physics of FLEM in RFP plasmas, because the FLEM instabilities in RFP possess the poloidal coupling mainly between non-resonant modes (with the rational surfaces outside the plasma) and presented a relatively simple physics. In tokamak plasmas the FLEM instability essentially has similar nature as studied in this section though the (dominant) non-resonant mode coupled with the resonant modes (with the rational surfaces inside the plasma). Only marginal differences come from the different configurations regarding with the EPs kinetic effects.

5.

3.1 Driving mechanism of FLEM

RFP magnetic configurations is characterized by the reversed toroidal magnetic field, which allows a RFP to operate in the parameter region where the resonant ideal kink modes appear to be stable. While the non-resonant external ideal kink modes could be strongly unstable due to the large plasma current, unless a surrounding perfect conducting wall is sufficiently close to the plasma surface. Therefore, the non-resonant external kink modes are the easiest to be excited modes among the kink mode spectrum of RFP plasmas.

It is interesting to find that, contrary to the RWM, FLEMs satisfy the usual external ideal kink dispersion relation:

$$-\delta I + \delta W_F + \delta W_{vb} + \delta W_k = 0 \qquad (18)$$

where δI represents the inertial energy component. The normalized Eq.(18) (by $\int \rho |\xi|^2 dx^3$) can be further written in the real and imaginary parts separately

$$(n\Omega - \omega_r)^2 - \gamma^2 = \delta W_F^r + \delta W_{vb} + \delta W_k^r = \delta W_b^r + \delta W_k^r \equiv \delta W_{bk}^r \qquad (19.1)$$

$$-2\gamma(n\Omega - \omega_r) = \delta W_k^i + \delta W_F^i \qquad (19.2)$$

where the superscript "*r*" denotes the real part of the energy components and "*i*' denotes the imaginary part. In the fluid theory (where δW_k=0) , $\delta W_b > 0$ indicates the external kink mode being stable with an ideal wall at r=b. Thus δW_b =0 set a stability boundary, beyond which, δW_b <0, the ideal wall can no longer stabilize the mode. The value of δW_b depends on the equilibrium parameters of the plasma. For a given current profile, the value of δW_b sensitively depends on the plasma beta value (β_p in RFP) and the wall proximity, expressed by the normalized minor radius of the wall i.e. r = b/a In fact, δW_b =0 corresponds to the so-called the "ideal wall beta limit" in the

RWM study, where the ideal non-resonant external kink modes stay near the marginal stability with an ideal wall. Furthermore, when the kinetic (wave –particle interaction) effects are taken into account, as shown in Eq.(19.1), the contribution of the kinetic energy component δW_k^r modifies the stability boundary of the ideal kink mode. This will be shown in the next figures.

The numerical analysis found that usually the imaginary part of δW_k is much larger than that of δW_f, i.e. $\delta W_k^i >> \delta W_F^i$, Therefore, Eq.(19) generally can be written as

$$(n\Omega - \omega_r)^2 = \frac{1}{2}\left[\delta W_{bk}^r + \sqrt{(\delta W_{bk}^2) + (\delta W_k^i)^2}\right] \qquad (20.A)$$

And $$\gamma = -\frac{\delta W_k^i}{2(n\Omega - \omega_r)} \qquad (20.B)$$

Moreover, it is found that in most parameter region of RFP plasmas, δW_b^r is a dominant term in δW_{bk}^r, and $\gamma << \omega_r$. The Eqs.(19) can be further approximated to

$$|n\Omega - \omega_r| \approx \sqrt{\delta W_b^r} \qquad (21.A)$$

$$\gamma \approx \frac{\delta W_k^i}{2\sqrt{\delta W_b}} \qquad (21.B)$$

Eq. (21.A) and (21.B) clearly indicates the FLEM physics: The kink mode frequency is mostly determined by the real part of the energy components δW_b, and the growth rate of the instability is mainly contributed by δW_k^i , which comes from the precession drift resonance of the trapped energetic ions. If the frequency ω_r falls inside the range satisfying the resonant condition with the precession frequency of a given type of EPs, i.e. $\omega_r - n\Omega \approx n\omega_d^a$, the instability of FLEM may appear. Therefore, the FLEM frequency ω_r directly links to the value of ω_{da}, and the plasma rotation provides a Doppler shift $n\Omega$ on the frequency.

Obviously, in the limit case, where plasma β_p reaches to the vicinity of the ideal wall beta limit, $\delta W_{bk} \approx 0$, and δW_k^i plays the major role in the dispersion relation, Eq.(19) results to

$$\gamma \approx |n\Omega - \omega_r| \approx \sqrt{\delta W_k^i / 2}\,. \qquad (22)$$

Fig.3 shows (a) the normalized growth rates and (b) the frequencies of FLEM instability as a function of β* in RFP plasmas computed by MARS-K code, only the kinetic effects from the precession drift motion of trapped EPs is taken into account in the calculation. The comparison has also been made between the results by directly solving the set of equations (1)-(5) from MARS-K code and that calculated by using the dispersion relation Eq.s (21); A good agreement is found and presented in the figure. In the plots, both the frequencies and the growth rates are normalized by ω_A, $\omega_A = B_o / (R_o\sqrt{\mu_o\rho_o})$. The birth energy ε_α of the hot ions from NBI is taken as ε_α=100ev. The EPs' beta fraction profile is taken as $\beta^*=\beta_o^*$. We take a fixed value of the total plasma poloidal beta, β_p=0.135, and the β* value varies from 0.0 to 2.0 (corresponds to the value of N* changing from 0 to 0.4591). Two cases, without plasma rotation Ω=0 and with rotation Ω/ω_A=0.05 are plotted. It shows that when β* overcomes a critical value $\beta^*_c \approx 0.28$ the FLEM instability appears with rather high frequency, which is in the range of the Alfven frequency. With increase of the β* value, the mode growth rate is enhanced due to the increase of the kinetic energy component δW_k^i . Nevertheless, the FLEM frequency remains almost invariant due to the fact that the value of δW_b remains invariant, because the total plasma beta β_p and the wall position b are unchanged. Since the birth energy ε_α , thus ω_{da} is the same for the two cases, with and without rotation, by following the condition of $\omega_r - n\Omega \approx n\omega_d^a$, the mode has a higher frequency with plasma rotation than the one without due to the Doppler shift $n\Omega$.

The value of δW_k^i is mainly determined by the two features of EPs: 1) the density fraction of EPs N_a/N_e, and 2) the birth energy ε_α, which directly links to the precession frequency ω_d^α. The parameter $\beta^*(=\beta_\alpha/\beta_{thermal})$ reflects the combination of these two effects. We note here that in contrary to the RWM theory, where the δW_k^i contributed from the kinetic resonant, as a damping factor, plays only a stabilizing role. While in FLEM the imaginary part of the kinetic energy component δW_k^i is the only possible driven mechanism for the instability.

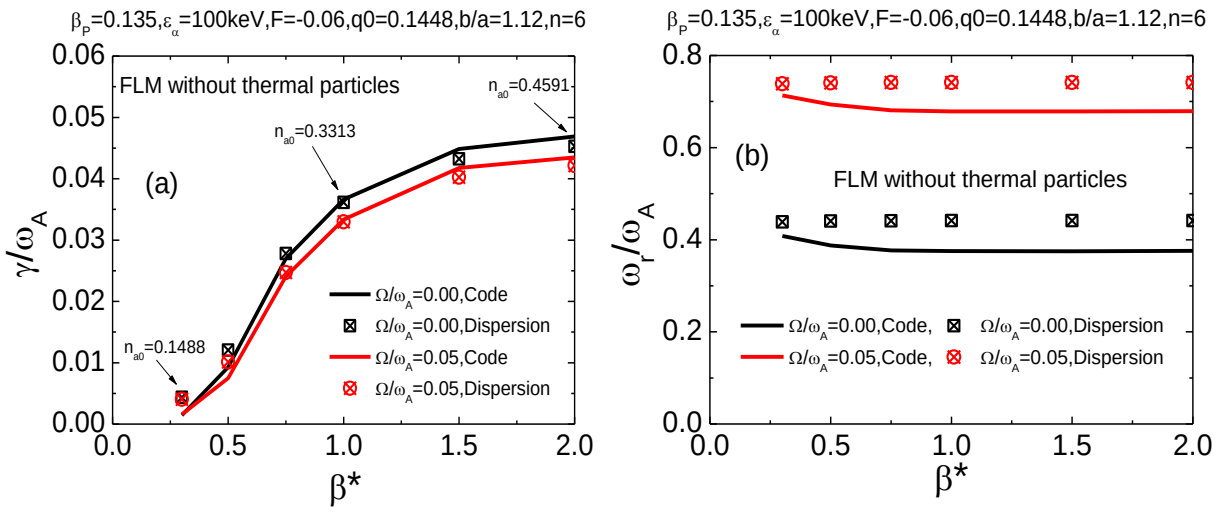

Fig. 3. plots of the normalized (a) growth rates γ/ω_A and (b) the real frequencies ω_r/ω_A of FLEM as a function of the beta fraction of the energetic particles $\beta^*=\beta_\alpha/\beta_{thermal}$. Two cases: $\Omega=0$ and $\Omega/\Omega_A=0.05$ are calculated. The comparison between the results from direct MARS-K computations and that by using the dispersion relation Eq.(21) is shown. The equilibrium parameters are chosen as: $\beta_p=0.135$, $b/a=1.12$, $F=-0.06$, $\varepsilon=a/R=0.23$, and $q(0)=0.1448$.

3.2 Excitation conditions of FLEM instability

The Eps can induce an unstable external ideal kink mode by the precession resonance under the two conditions: 1) the sufficient fraction of the trapped EPs. (2) The range of the kink mode frequency ω_r can match the resonant condition $\omega_r - n\Omega \approx n\omega_{da}$.

As regard to the effect of the EPs' fraction on the FLEM instability, the important measurement is their contribution to the imaginary part of the kinetic energy component δW_k^i as indicated in the dispersion relation Eq.(21.B). Since the value of δW_k^i contributed from EPs is promotional to the value of P_a, both density fraction N_a* and the birth energy ε_α can influence δW_k^i via P_a. Besides, a more important fact is the value of ε_α , which directly relates to the EPs' precession frequency ω_{da}, thus sensitively affects the resonant condition and the kinetic resonant energy component δW_k^i. We find that though both N_a and ε_α can influence the value of β*, the birth energy ε_α affects the FLEM instability nature with higher sensitivities. Fig.4 shows the normalized mode growth rates and frequency versus the density fraction of EPs for two different birth energies ε_α=100 ev and ε_α=80 ev. The EPs with a higher birth energy can drive FLEM instability at much lower critical β* value and low density fraction. For the same β* value, the higher birth energy leads to the higher growth rate. The mode frequencies are almost same for the two cases due to the same β_p value for the two ε_α cases.

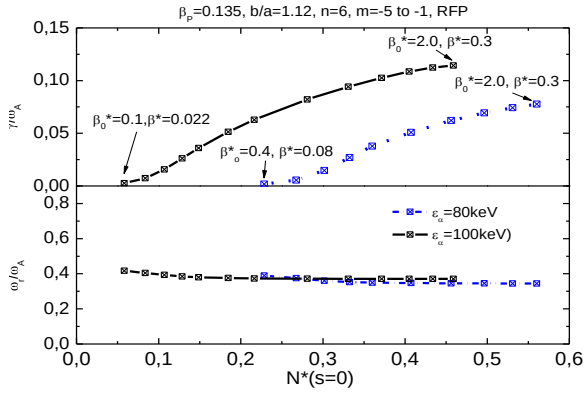

Fig.4 growth rates and frequencies of FLEM instability are plotted as a function of the density fraction of Energetic ions $N^*(s=0)=N_\alpha/N_{th}$ for two different birth energies ε_α=80ev (dotted lines)and ε_α =100ev(solid lines). The values of β^* and β_o^* corresponding to the starting and ending points of the curves are marked in the figure. βp=?

The total plasma beta value significantly influences the behavior of FLEM instability. In Fig.5 the growth rates and the frequencies of FLEM instability as a function of the total plasma poloidal beta β_p are shown in (a) and (b) respectively for the birth energy ε_α=100kev. Four different considerations of the kinetic resonant effects are presented: (1) The kinetic effects contributed by only hot ions with β_o^*=0.3 (β^*=0.062) (2) by only hot ions with higher EPs fraction β_o^*=1.0 (β^*=0.176), (3)contributed by both hot ions and bulk thermal particles β_o^*=1.0 (β^*=0.176) (4) by the usual thermal particles only (without hot ions), thus the FLEM instability disappears; And only a RWM instability can be found if the wall is a resistive one. When the wall is an ideal one, only the ideal kink instability exists in the region where the value β_p beyond the ideal wall beta limit, β_p^{ideal}. This is presented in curve (5). Comparison between the case (1) and (2) indicates that EPs with higher β^* (implies higher density fraction N*) can drive FLEM instability in wider region, which extends to smaller β_p value, and have higher growth rates. In case (3) we take into account the kinetic effects of the thermal bulk particles. It is found that the unstable region becomes smaller, due to the cancellation of the kinetic contributions to δW_k^i between the driving mechanism of the precession resonance of EPs and the damping effect of the transit resonance of the thermal particles. In another word, the ion acoustic Landau damping of the thermal ions play a stabilizing role on FLEM.

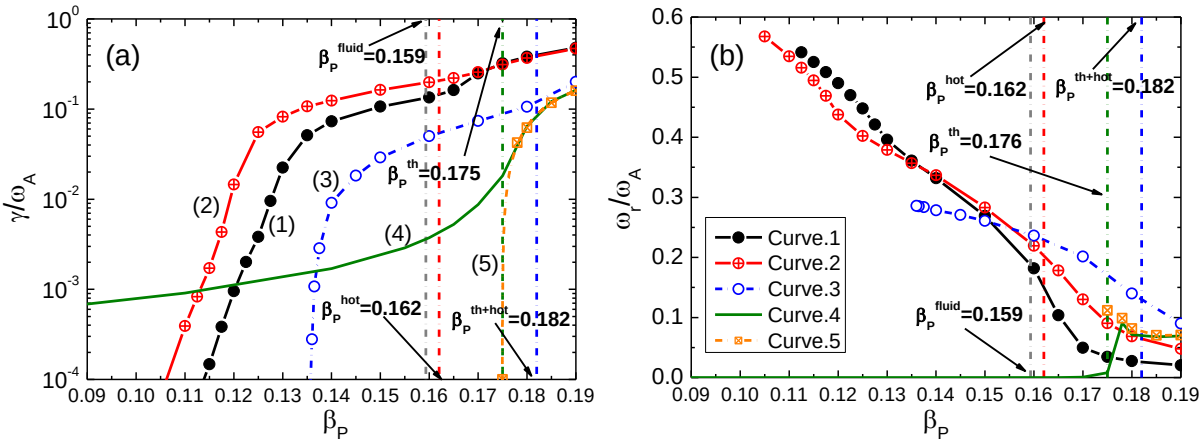

Fig.5 The Growth rates(a) and the frequencies(b) of the n=-6 FLEM instabilities plotted as a function of the plasma poloidal beta β_p for different β^* values of the energetic particles with birth energy ε_α=100kev. Comparison made for 5 cases: Curve (1) and (2): only consider the kinetic contribution of EPs with β_o^*=0.3(β^*=0.062) and β_o^*=1.0 (β^*=0.176) respectively, Curve (3): the kinetic contribution from both EPs and bulk thermal particles are considered β_o^*=1.0 (β^*=0.176). Curve (4) and (5), without EPs, only thermal particles are involved in computation, with a resistive wall (penetration time scale τ_w/τ_A=4.4x10^3), and an ideal wall respectively. b/a=1.12, F=-0.06, q_o=0.1448.

The upper-bound of the FLEM instability interval appears at the region $\beta_p \approx \beta_p^{ideal}$ ($\beta_p \le \beta_p^{ideal}$), where the external kink mode is near marginal stability and has lowest frequency resulted from small δW_b. For given EPs (β^*, ε_α), when β_p decreases, the value of fluid potential energy component $|\delta W_F|$ (δW_F <0) decrease due to reducing the pressure driven effects, and resulting to a larger δW_b ($\delta W_b = \delta W_F + \delta W_{vb}$, $\delta W_{vb}>0$). Therefore, ω_r increases. When β_p comes down to sufficient low value, and ω_r becomes too high to meet the requirement of the resonance condition, EPs cannot contribute enough driving energy δW_k^i, so FLEM disappears.

The vertical lines in figure 5 represent the ideal wall beta limits for various cases mentioned above. The contribution of the kinetic effects can modify the ideal wall beta limits predicted by the fluid theory, which has been observed experimentally [25]. In figure 5, we also indicate that the ideal wall beta limits β_p^{ideal} are significantly influenced by the various kinetic effects. As marked in the figures, the fluid theory predicted the minimum value of β_p^{ideal}, noted as β_p^{fluid}=0.159 (corresponds to δW_b=0); the kinetic effects from only energetic particles shift the value near to β_p^{hot}=0.162 (corresponds to δW_{bk}=0); the effects of only kinetic thermal particles move the value to β_p^{th}=0.175; when taking into account the kinetic effects from both hot ions and thermal particles, the value shifts to the maximum as β_p^{th+hot}=0.182.

Fig.6 presents the radial profiles of the various frequencies averaged over poloidal angles and velocity space for the curve(3) of Fig.5. The precession frequencies of the EPs and the transit frequencies of the thermal ions for three different β_p values (βp=0.14, 0.16, 0.18) are presented. The

shaded area presents the frequency range corresponding to full unstable region for curve (3) of Fig.5. The plot confirms that both EPs precession resonance and transit resonance of thermal ions can occur and play significant roles to FLEM instability.

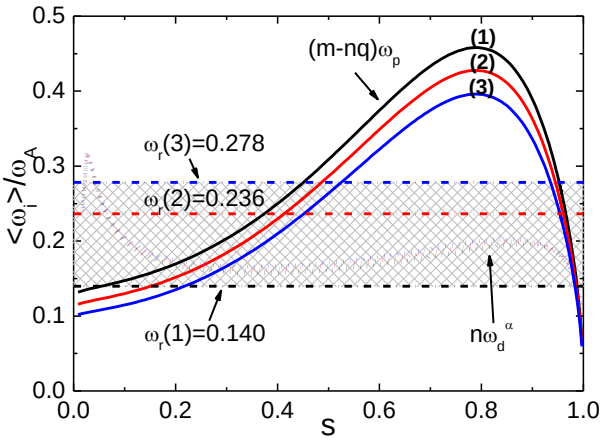

Fig.6 the precession frequencies of Energetic ions ω_{da} and the transit frequency of the thermal ions $(m\text{-}nq)\omega_p$ corresponding to different β_p values, β_p=0.18(1), 0.16(2), 0.14(3), are shown for RFP plasmas, and compared with the FLEM frequencies. The shaded area presents the frequency range corresponding to the unstable FLEM region of curve (3) in Fig.5 , where the kinetic effects of both EPs and thermal particles are considered.

In Fig.7 we plotted the unstable region of FLEMs on the β_p-b/a plane for two different birth energies of the energetic ions. The solid (black) line represents the ideal wall beta limit, while the dashed (red) line (ε_α=100ev) and the dotted (blue) line (ε_α=150ev) represent the lower-bounds of the unstable regions. No plasma rotation is considered. The shaded area represents the unstable FLEM region. It shows that the higher β* value (higher birth energy ε_α in this case) results to a larger unstable parameter region. For a given wall position b/a

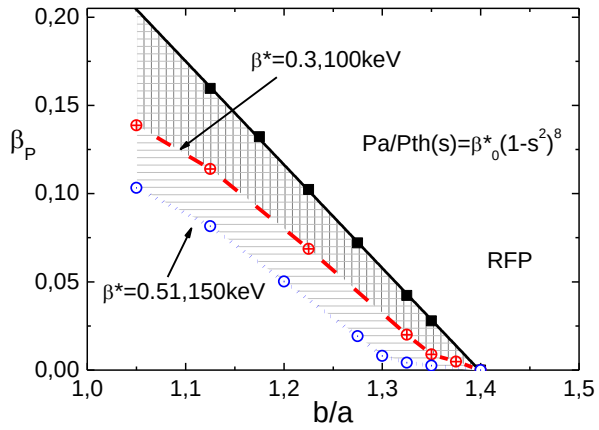

Fig 7. The unstable region of the n=6 FLEM is plotted in the plane of the poloidal beta β_p versus the wall position b/a. The solid line with square points represents the ideal wall beta limit, which is also the upper-bound of the beta value for the Instability; while the other two lines (dashed line and the dotted line) represent the lower-bounds of the instability

window for the two cases: β_o=0.3 ε_α=100kev and β_o*=0.51 and ε_α=150kev. The other equilibrium parameters are F=-0.06, q0=0.1448, and Ω=0.*

the shaded βp interval exists, where the discrete external ideal kink mode possesses appropriate frequency ω_r ,which can resonant with the precession motion of EPs. Similarly, for a fixed β_p value, an interval of the wall position b/a also exists.

3.3 The role of the surrounding wall on the FLEM instabilities.

Due to the FLEM instability has rather high frequency, the usually existing resistive wall in experiments plays a role of an ideal wall for FLEM. In fact, it is found that the instability appears independently from the wall resistivity in most resistivity range. For extremely high resistivity wall, the FLEM may connect to the branch of the no-wall ideal kink instability. However, the wall position can give a strong influence on the FLEMs. In figure 8, we plot the mode growth rates and frequencies as a function of the wall position b/a for different EPs birth energies ε_α and plasma poloidal beta values βp. The comparison is made between a resistive wall and with an ideal wall bounderies. The lines in the figure denote the results with an ideal wall, while the dots represent the results with a resistive wall having a normalized penetration time scale as τ_w/τ_A= *4.4×10^3* .

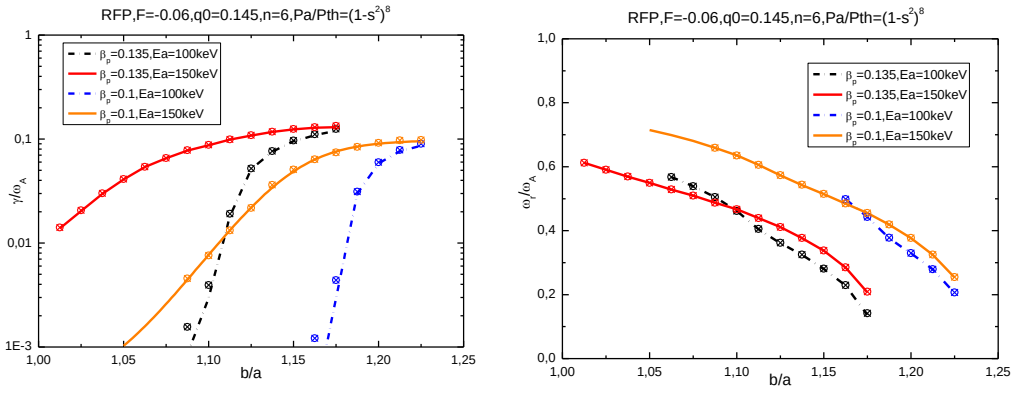

Fig.8 plot of the growth rates and the frequencies of n =-6 FLEM instability vs. the normalized wall position b/a computed by MARS-K. The lines represent the results with an ideal wall and the dots represent the results with a resistive wall having penetration time scale equal to τ_w/τ_A= 4.4×10^3 . The other parameters are the same as in Fig.7

The ideal wall and the resistive wall give almost the same results. The wall being closer to plasma could set more serious condition for the FLEM excitation. In the lower βp case, βp=0.1 , The ranges of the wall position b/a for FLEM instability are b/a=1.16-1.225 for ε_α=100kev and b/a=1.05-1.225 for ε_α=150 kev respectively. Obviously, the EPs with higher ε_α can extend the instability to smaller

b/a. For higher βp case, βp=0.135, the instability region of b/a extents to the vicinity of the plasma surface.

3.4 The kinetic effects of the thermal particles on FLEMs

The kinetic effects of the thermal particles play a stabilizing role on the FLEM instability, which has be shown in the subsection 3.2, in Fig.5 , curve (3). It indicates that by taking into account the kinetic effects of thermal particles, the instability requires higher βp value and has the lower growth rates than that by considering the EP's kinetic effect alone. The kinetic damping effects are mainly contributed by the transit resonance of the passing ions. As shown in Fig.6, the transit frequency of the passing ions is comparable with the precession frequency of the EPs; and both can resonant with the FLEMs. However, the contribution to the imaginary part of the kinetic energy from thermal particles partially cancels the contribution from EPs, thus the thermal particle play a damping role on FLEM instability. In Figure 9, we plotted the perturbed energy components (normalized by $\int \rho|\xi|^2 dx^3$) corresponding to the point of β_p=0.14 in Fig.5 and two cases (with and without kinetic thermal particles) are compared for the same β* values, β*=1.0: In the first group of the energy columns only the kinetic contribution of hot ions is considered (corresponds to the case (2) in Fig.5). In the second group of the energy columns, both kinetic effects from hot ions and the thermal particles are included (corresponds to the case(3) in Fig.5). In each group, the first column represents the fluid contribution of δW_b, second column is $\delta W_{bk}=\delta W_b+ \delta W_k^r$. Third is δW_k^r and fourth is the imaginary part of kinetic energy δW_k^i. It shows the value of δW_k^i in second group dramatically decreases with respect to the first group, while other components have only minor changes. This implies that the kinetic damping of the thermal bulk particle cancels the kinetic driving effects of the hot ions, leads to smaller growth rates and narrower parameter region of FLEM instability. In addition, It is easy to be understood that the mode frequency becomes slightly lower due to the modification made by δW_k^r on δW_b, ($\delta W_{bk}<\delta W_b$).

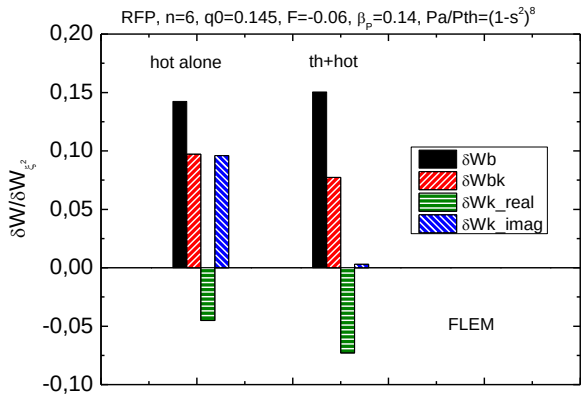

Fig.9 Comparison of the energy components between the two groups: first group represents the results where only kinetic effects of the hot ions are considered in the computation. The second group involved the kinetic effects of hot ions and the full kinetic effects of the thermal particles. The parameters used as the same as in Fig.5 at point of β_p=o.14 and β_0=1.0.*

In Fig.10, (a) the imaginary parts and (b) the real part of the kinetic energy components are plotted as a function of plasma toroidal beta β_p, corresponding to the curves (3) of Fig.5. In Fig.10(a), It shows that the significant cancelation occurs in the whole unstable region for the imaginary part δW_k^i between the contribution of the hot ions and the bulk thermal ions. This implies that the ion Landau damping by the thermal particles plays a stabilizing role for the FLEM instabilities. Fig.10(b) indicates that the kinetic resonance provided by the thermal particles also slightly modify (cancel) the contribution to the real part of δW_k^r from the energetic ions , resulting to the modification of the mode frequencies.

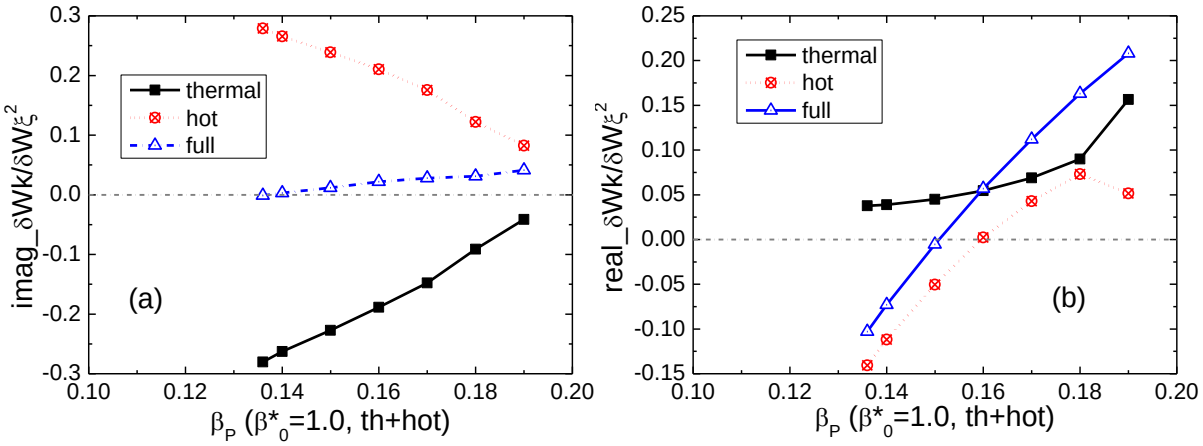

Figure 10. The kinetic energy components δW_k versus the poloidal plasma beta β_p are plotted with β_o =1.0, β*=0.176 , corresponding to the case (3) of the figure 5. The analysis is made for 3 cases: kinetic energy component contributed from the hot ions (marked "hot"), from the thermal particles (marked "thermal"), and contributed from both hot and thermal together ("full"). a) the imaginary part δW_k^i . (b) the real part δW_k^r .The other parameters are same as that in the figure5.*

3.5 Relation with the RWMs

Fish-bone like external kink mode can co-exist and/or couples with Resistive Wall Mode. Both modes are originated from the ideal external kink, which is stable in the plasmas with a sufficiently closed ideal wall. The RWM instability is caused by the replacement of the ideal wall with a resistive wall, which allows the penetration of the perturbed magnetic field; while the FLEM instability is driven by the precession motion of trapped energetic particles, which resonates with the external kink mode.

Fig.12 shows the normalized mode growth rates γ/ω_A and frequencies $\omega_r/\ \omega_A$ of both FLEMs and RWMs as functions of the plasma rotation frequency $\Omega/\ \omega_A$, for various β* values of EPs; while the

beta value of the thermal particles $\beta_{thermal}$=0.015 remains invariant. Only the kinetic effects of hot ions are considered here. Part (a) shows the negative rotation (Ω<0) cases, where the Doppler shift leads the value of the FLEM frequency decreasing with the rotation. Further increase $|\Omega|$, ω_r crosses the zero (in the vicinity of RWM frequencies), and becomes negative. The FLEM instability remains unstable when the plasma rotation increases because the condition of $\omega_r - n\Omega \approx n\omega_{da}$ is satisfied. The RWM instabilities, instead, are damped by the same motion of the hot ions, and become stable with the negative rotation, where the same resonance of ω_r-nΩ-n$\omega_{da} \approx 0$ ($\omega_r \approx 0$ for RWM) can be satisfied. The figure shows two unstable modes (FLEM and RWM) generally can coexist. In the particular case of β^*=2.13, β_p=0.040, at the rotation $\Omega/\omega_A \approx$ -0.047, the coupling of the two modes appears, since both the frequencies and the growth rates of the two modes are very close to each other. The positive rotation case is presented in (b), where the ω_r of FLEM increases rapidly with rotation due to the Doppler shift, and cannot be vanish. The RWM cannot be stabilized by kinetic effects of EPs alone, the stabilization can be reached if the ion acoustic continuum damping by the thermal particles is taken into account [26], which is not the case of present figure. The coupling of the two modes has not observed due to the large differences in both the frequency and growth rates. Therefore, only the coexistence is presented in the figure.

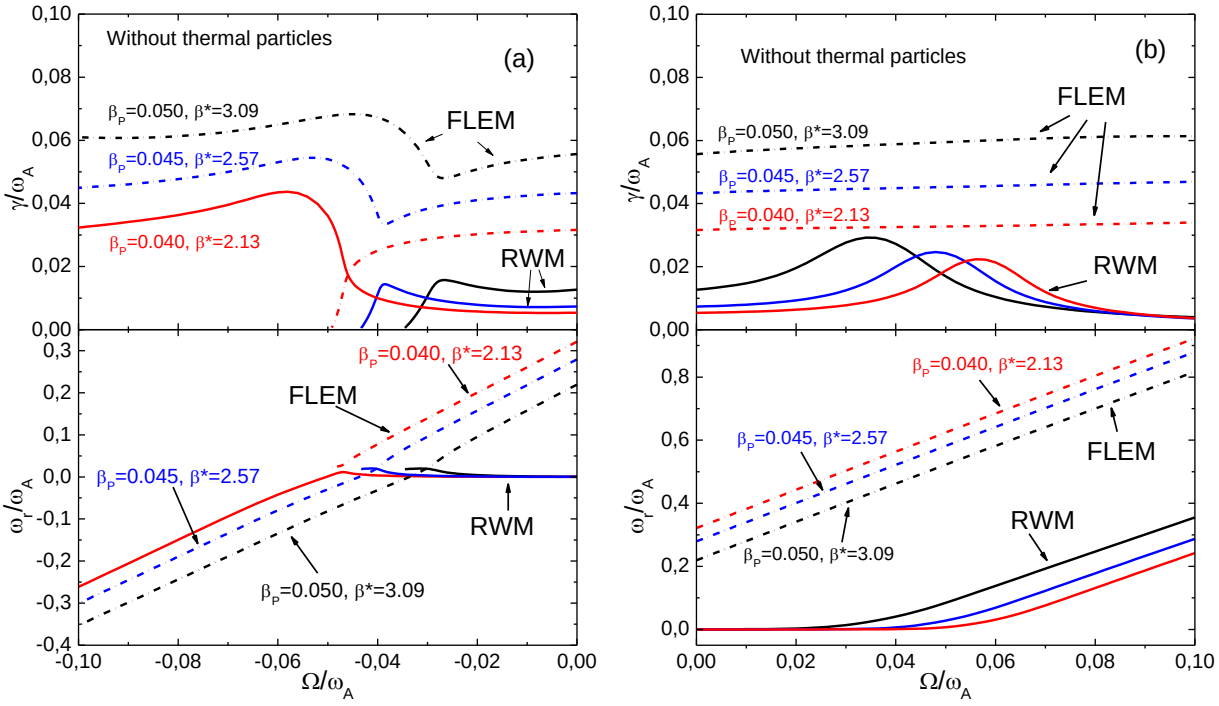

Fig. 12 The normalized growth rates and the frequency of the RWM and the FLEM (co-existing and coupling, n=6), are plotted as a function of the normalized plasma rotation frequency Ω/ω_A for β^* =3.1 (β_P =0.05), β^* =2.6 (β_P =0.045)

and β^* =2.1 (β_P =0.04) with the unchanged thermal poloidal beta $\beta_{thermal}$ =0.015. The model of β^*=const. for pressure fraction of EPs has been used in the computation. b/a=1.275 and ε_α=100keV, F=-0.015 and q(0)=0.145.

Fig.13 compares the eigenfunctions of FLEM and RWM, where only the kinetic effects of hot ions are considered. ξ_1 denotes the displacement of the modes in the radial direction and Q_1 denotes the radial component of the perturbed magnetic field. The data are taken as $\beta_0^* = 1.0$, βp=0.12, and without rotation. The penetration time scale of the wall is taken as $\tau_w/\tau_A = 4.4 \cdot 10^3$. It shows that the two "external kink" originated modes have rather similar shapes of the eigenfunctions for both ξ_1 and Q_1. Nevertheless, the eigenfunctions of FLEM have been pushed toward to the plasma core by the wall, clearly show almost vanished Q_1 at the wall position. The eigenfunction Q_1 of RWM , instead, penetrates through the wall and extends to the vacuum region. Therefore, the wall for RWM ($\omega_r/\omega_A \approx 0$) is a resistive wall and allows the magnetic perturbation penetrating. For FLEM (with $\omega_r/\omega_A \approx 0.48$), however, it works as an ideal wall.

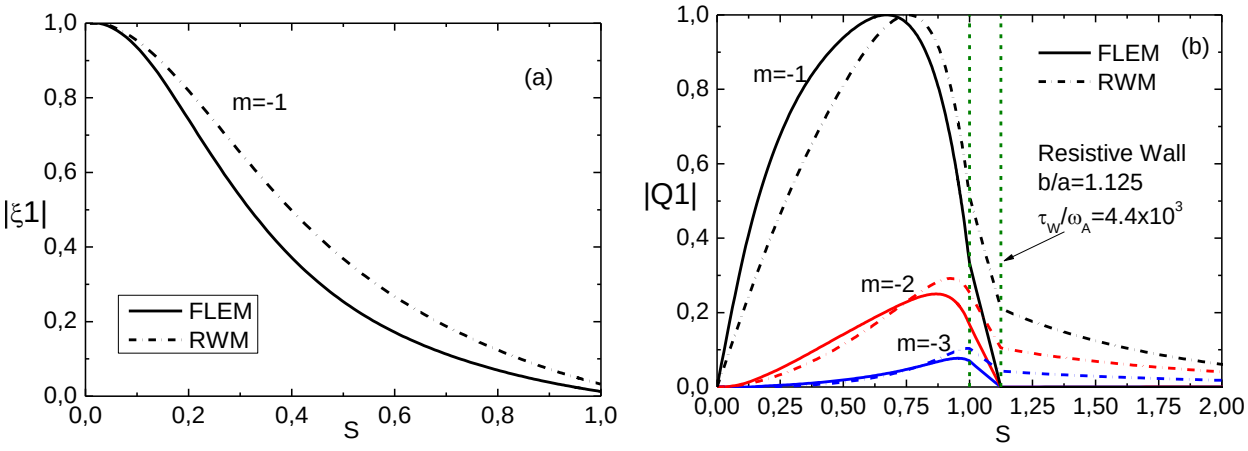

Figure 13. The absolute values of the dominate components of (a) the radial plasma displacement $|\xi_1|$ (n=6, m=-1) and (b) the radial perturbed magnetic field $|Q_1|$ (n=6, m=-1,-2,-3) are plotted along the minor radius for the FLEM and the RWM. s=1 corresponds to the plasma edge, and wall locates at b/a=1.125. Only the kinetic effects of hot particles are considered and without the plasma rotation. β^*_o=1.0, β_p=0.12. The poloidal Fourier harmonics are taken from m=-5 to -1 for computation. The other parameters are chosen as the same as Fig.5.

4. FLEM instability in Tokamaks

4.1 Excitation of FLEM instability

The FLEM instability can be driven in Tokamak by the same mechanism. The modes show a similar nature with what studied in RFPs. Nevertheless, the FLEM driven by EPs in tokamaks has

much lower frequencies than that in RFPs (with the same birth energy ε_α). The reason is that the tokamak configuration has the larger scale length of magnetic gradient and curvature radius (order of major radius R) than that in RFP configuration (order of minor radius r), resulting in the lower precession frequency of hot ions in Tokamak than in RFP. Besides, the Landau damping by the bulk thermal ions in RFP would be relatively stronger than in tokamak due to the shorter connection length in RFP than in tokamaks.

Figure 14 shows the growth rates and frequencies of n=1 FLEM instability versus the total plasma beta β in the circular tokamak(similar geometry as the RFP in previous section) with q(0)=1.14 , q(a)=3.68, and b/a=1.12. The poloidal harmonics are taken from m=-10 to 5. The parameters of the energetic ions with ε_α=100kev are taken similar as in Fig.5. Three cases are studied: (1) β_0*=0.3(β*=0.067) and (2) β_0*=1.0 (β^*=0.19), where only the kinetic effect of EPs are considered; case (3) β_0^*=1.0 (β^*=0.19), the kinetic resonances from both EPs and bulk thermal particles are taken into account. The figure shows the similar behaviors of FLEM instabilities as what shown in Fig.5 for RFPs: The FLEM in Tokamak can also be triggered by EPs, when the plasma beta β exceeds a critical value, which depends on the fraction (β*) of the EPs. The comparison between case (1) β_o^*=0.3 and (2) β_o^*=1.0 indicates that the higher fraction of EPs leads to the lower critical β value, and higher growth rates. The real frequencies ω_r / ω_A of the FLEM, which are linked to the precession frequency of EPs, are also reduced by increasing the plasma beta. Nevertheless, the values of ω_r are much smaller than those for RFPs. The thermal ion landau damping also plays a stabilizing role, which can be observed by comparing case (2) (kinetic effects of hot ions alone) and case (3) (kinetic effects of hot plus thermal ions). In the Tokamak, the poloidal harmonics of FLEM can be non-resonance and/or resonance, where the dominant non-resonant external kink mode (e.g. m=-1, n=1) couples with the resonant external kink modes (e.g. m=-2, -3, n=1). The no-wall β limit $\beta_{limit}^{nowall} = 0.0078$ (β_N^{nowall}=2.11) and the ideal wall β limits β_N^{ideal} for various cases are marked in the figure. Similarly as shown in RFP case(Fig.5) the value of the ideal wall beta limit is modified by the kinetic effects: $\beta_{limit}^{idealwall} = 0.0124$ ($\beta_N \approx 3.34$) for EPs kinetic effect alone and $\beta_{limit}^{idealwall} = 0.0139$ for full kinetic (both EPs and thermal ions) effects. Here β_N is defined as $\beta_N = \beta_T(aB_T/I)$, $\beta_T = 2\mu 0\langle p\rangle/B_T^2$, $\langle p\rangle$ is the average plasma pressure, μ_0 is the vacuum permeability and B_T is the strength of the toroidal magnetic field.

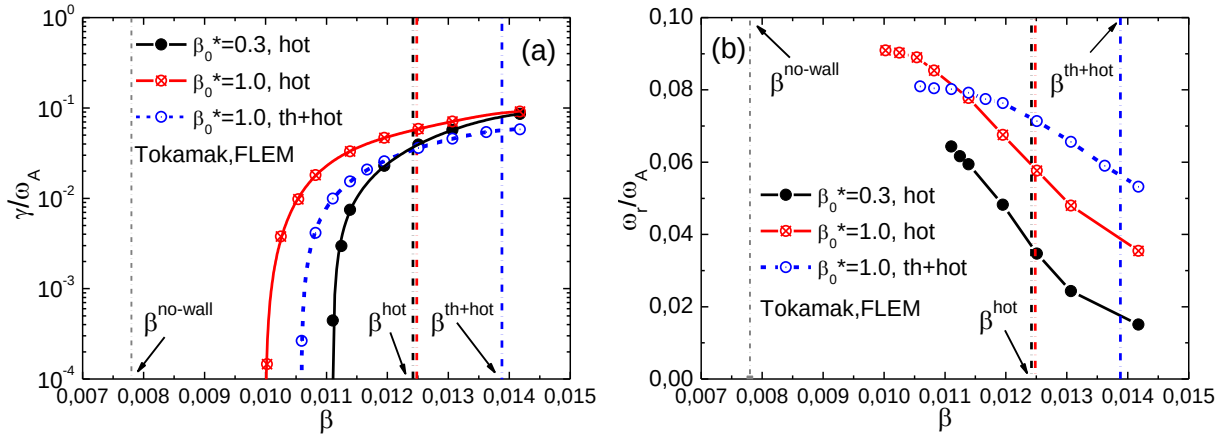

Fig.14 The n=1 FLEM (a) growth rate γ/ω_A and (b) real frequency ω_r/ω_A versus the plasma beta β value are plotted. The solid lines represent the kinetic effects contributed only by the EPs for two different fractions β_o^*=0.3(β=0.067) and β_o^*=1.0 (β*=0.19) respectively. The dashed line represents the results where the kinetic contribution from both EPs and thermal ions are considered, with β_o^*=1.0 (β*=0.19). b/a=1.12, Ω=0 and ε_α=100kev.*

The general dispersion relation for external kink mode of Eq.(20) can still apply to the Tokamaks. However, the dispersion relation of Eq.(21), which under the approximation of $\omega_r >> \gamma$, is no longer valid since the values of ω_r are comparable with γ in tokamaks. Thus the kinetic energy component δW_k introduces an additional influence on the mode frequency ω_r.

The 2-D plots show in Fig.15 (a) is the precession frequencies of the EPs $n\omega_{da}$ (averaged over the velocity space), and (b) the imaginary parts of the kinetic energy δW_k^i for FLEM in tokamak plasmas .Only the kinetic effects of hot ions are taking into account here. The parameters taken for this computation are β=0.012 (β_N=3.02) and β_o^*=1.0, β*=0.19; the corresponding point can be found in Fig.14 case (2). The Fig.15(b) shows that the main contribution to the kinetic energy δW_k^i comes from the region close to the magnetic axis of the low field side, corresponds to the area of $n\omega_{da} \approx$ 0.015-0.06 in(a), which is in the vicinity of the FLEM frequency $\omega_r/\omega_A \approx$ 0.065 obtained in Fig.14 for β =0.012. Thus, the δW_k^i is contributed by the interaction of EPs with the external kink through the precession resonance. We notice that the values of $n\omega_{da}$ which provide maximum contribution to the kinetic energy δW_k^i do not completely well coincide with the mode frequency ω_r. This discrepancy may be due to the fact that, the plot of $n\omega_{da}$ in (a) is made by the average over the velocity space, which can only give a

rough ideal about the averaged value of ω_{da}, cannot always exactly describe the resonance process.

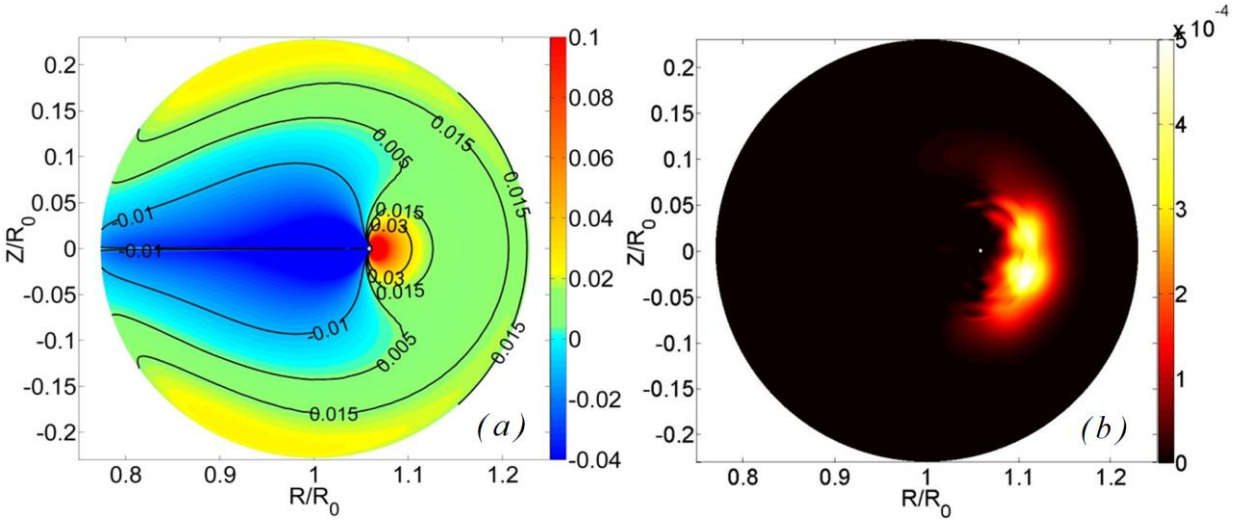

Fig. 15. The 2-D plots of (a) the precession frequency of the EPs $n\omega_{da}$ (averaged over the velocity space), and (b) the imaginary parts of the kinetic energy component δW_k^i for the FLEM, with the plasma beta β=0.012 (β_N=3.02) and the fraction β_o^*=1.0 (β*=0.19) are shown in the R-Z plane. The other equilibrium parameters are chosen as Fig.14.

The unstable regions for n=1 FLEMs on the plan of the total plasma β vs. wall position b/a are shown in Fig.16 for $\beta_0^* = 0.3$ ($\beta^* = 0.067$), $\varepsilon_\alpha = 100keV$ and $\beta_0^* = 0.51$ ($\beta^* = 0.107$), $\varepsilon_\alpha = 150keV$ respectively. The instability area appears above the no-wall beta limit (marked in Figure as β^{nowall}=0.0078) and below the ideal wall beta limit. The latter is the upper-bound of the unstable region. The EPs with higher birth energy and/or higher fraction β* lead to a larger unstable area. The plasma with a closer surrounding wall requires higher beta value to excite the FLEMs. Furthermore, the figure indicates that the kinetic effects modify the ideal wall beta limit, thus the upper-bound of the unstable region. Beyond this limit, the ideal kink mode is intrinsically unstable whatever without/with the kinetic effects of EPs.

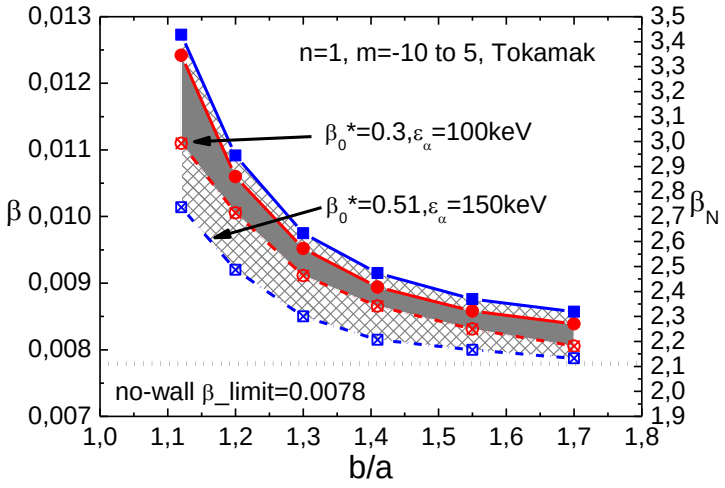

Figure 16. The unstable regions of the n=1 FLEM are plotted in the plane of the plasma beta β (left) and β_N (right) versus the wall position b/a. The horizontal dashed line represents the no wall beta limit (β^{nowall}=0.0078). Two different EPs parameters are compared: β_o^*=0.3(β^*=0.067), ε_α=100kev, and β_o^*=0.51 (β^*=0.107), ε_α=150kev. The shaded areas are the FLEM unstable area. In both cases, the solid lines denote the ideal wall beta limit modified by the kinetic effect, and the dashed lines denote the stable/unstable boundary of the FLEMs. No plasma rotation is considered.

4.2 Co-existence of FLEM and RWM

The co-existence of RWM and FLEM can also be observed in tokamaks,which is shown in Fig.17 , where both positive and negative directions of the rotation have been investigated, and the kinetic effects for trapped hot ions, trapped thermal particles are considered in the computation. For the FLEM instability, since the frequency should be determined by the resonance condition $\omega_r \approx \omega_{da}+n\Omega$, the positive plasma rotation increases the mode frequency, and the negative rotation decrease the frequency. However, the rotation does not significantly influences the growth rates of FLEM in both directions provided the resonance condition satisfied. For RWM instability, the mode frequencies are much lower than FLEM. In the positive rotation $\Omega > 0$ region, RWM can be stabilized by the kinetic damping contributed by the precession drift of the thermal trapped electrons [18, 27-29] at a very slow rotation velocity ($\Omega/\omega_A \leq 0.014$ as shown in Fig.17); and no resonance-stabilizing effects comes from the EPs. In the negative rotation $\Omega < 0$, both hot ions and thermal ions contribute to the kinetic energy δW_k^i. The RWM can be stabilized in the relatively slow (or vanish) negative rotation mainly by the contribution of the thermal trapped particles. When the rotation becomes more negative the RWM can be stabilized again mainly by the kinetic damping of the hot ions. We would discuss these RWM phenomena in detail elsewhere. Therefore, the figure presents a coexistence of the unstable FLEM and RWM. In the parameter region we investigated, there is no mode coupling observed, this may be due to the fact that the role of the negative plasma rotation frequency nΩ, (n=1) in tokamak could not decrease the FLEM frequency such rapidly as in

RFP where n=6, thus, before the FLEM frequency going down and reach the RWM frequency (near zero), the RWM has already stabilized by the kinetic damping of the EPs.

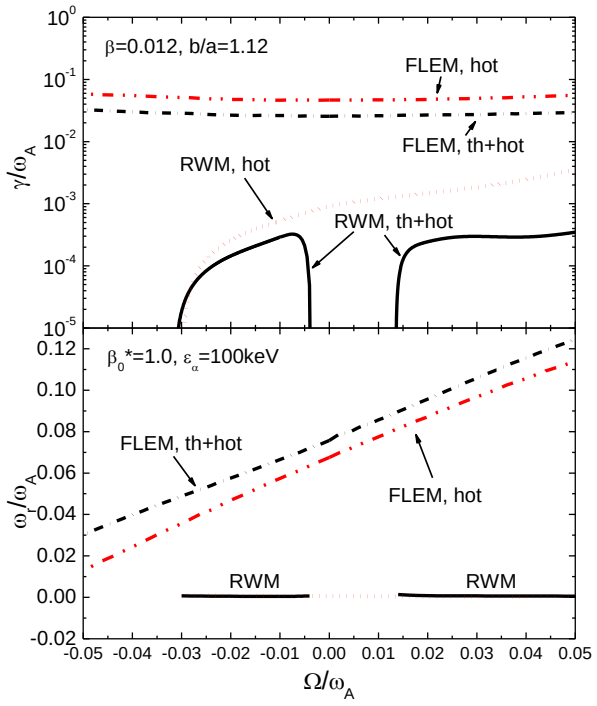

Fig. 17. The normalized growth rates and the frequencies of the co-existing RWM and the FLEM are plotted as a function of the plasma rotation frequency. The mark "hot" denotes the case where the kinetic effects contributed only by hot ions; "th+hot" denotes by both hot ions and thermal trapped particle. The parameters are taken as β_o^*=1,0 (β^*=0.19), β=0.012, , b/a=1.12 and ε_α=100kev.

The eigenfunctions of the co-existing FLEM and RWM are plotted in Fig.18, the radial displacements $|\xi_1|$ (absolute value) for most important poloidal modes (n=1, m=-1 to -4) are presented in (a) and the radial components of perturbed magnetic field $|Q_1|$ are presented in (b). The taken parameters correspond to the two coexisting modes shown in Fig.17 at the rotation frequency Ω/ω_A=0.2, The kinetic effects contributed from both hot ions and thermal trapped particles are considered (the curves marked with "th+hot" in Fig.17). The figure presents both non-resonant poloidal harmonic n=1,m=-1,-4 and resonant harmonics n=1,m=-2,-3. Similar to RFP cases, the eigen-functions of FLEM and RWM have similar shapes in general. However, the eigenfunctions of FLEMs are pushed toward to the plasma center due to the "ideal-like" wall, and show lower amplitudes of the displacements with respect to the one of the RWMs. The $|Q_1|$ of FLEMs vanish when reach the wall; while for the RWMs |Q1| can penetrate through the resistive wall and extend to the vacuum region.

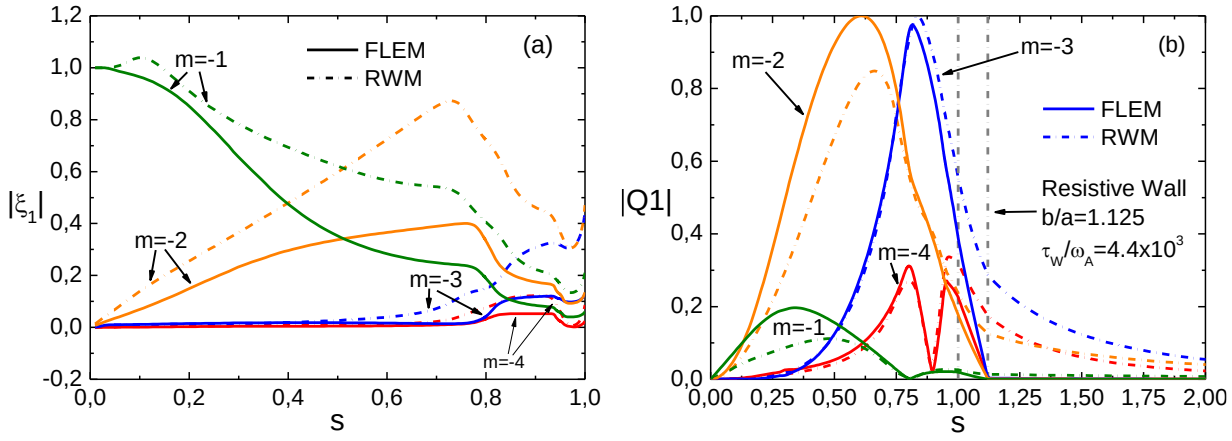

Figure 18 The radial components of (a) the plasma displacement $|\xi_1|$ and (b) the perturbed magnetic field $|Q_1|$ (n=1, m= -1 to -5) are plotted along the minor radius for the FLEM and the RWM, corresponding to the point in Fig.17 (full kinetic case) with the plasma rotation $\Omega/\omega_A = 0.02$. The total poloidal Fourier harmonics taken in the computation are m= -10 to 5. The other parameters are chosen as the same as in Fig.17

4.3 Damping by thermal particles

Similarly as in RFP plasmas, the thermal passing ions provide ion acoustic Landau damping on FLEMs instabilities also in tokamak. Fig.19 shows the various energy components, in particular, the imaginary part of the kinetic energy δW_k^i contributed by different species: energetic particles, the thermal particles and both together.

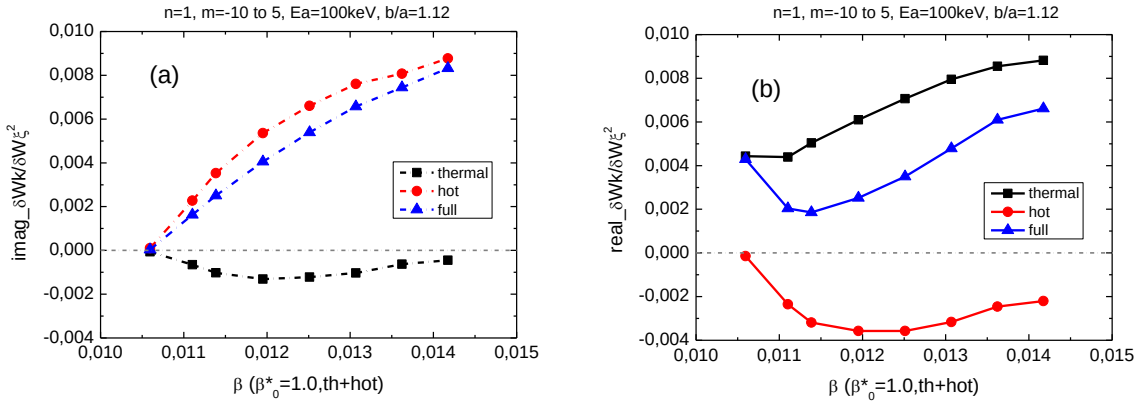

Figure 19. the kinetic energy components δW_k^i *and* dW_k^r versus the plasma beta β computed by considering kinetic resonances of both EPs and thermal particles are plotted, which corresponds to the curve "th+hot" in Figure 14. The contributions to δW_k by various species are presented: the curve "thermal" denotes the contribution of the thermal particles. " hot" denotes the contribution by energetic ions. "full" denotes the combination of the two species. The parameter used are the same as Figure 14 for curve 'th+hot", where β_o^*=1.0 (β*=0.19). (a) is the plot of imaginary part of the kinetic energy δW_k^i and (b) the plot of the real part δW_k^r.

The figure shows that the kinetic effects of thermal particles (passing ions) contributes to δW_k^i with the opposite sign of the contribution from EPs, and lead to cancelation to the driving force provided by EPs. Therefore, considering the kinetic effects of the thermal particles in tokamak, the FLEM instability becomes weaker with respect to the case of considering the hot ions alone (requires a higher β value for instability and results to a lower growth rate, as shown in Fig.14). However, the damping of thermal particles on the FLEMs in tokamaks seems not give a significant modification on driving effects from EPs; the cancellation of the thermal particles by their negative δW_k^i is relatively smaller than the RFP plasmas. The comparison between Fig.19 and Fig.10 (for a RFP) supports this conclusion. This is due to the fact that RFP configuration has shorter connection length than tokamak one, usually one observes a stronger Landau damping by thermal passing particles than what in tokamaks. This fact has also observed in the studies of other type of instabilities[30-32] in RFP plasmas.

7.Summary and discussion

In this paper, The fish-bone like external kink mode (FLEM) instability driven by the precession drift motion of the trapped Energetic Particles is numerically investigated for both RFP and Tokamak (circular cross section with similar geometry) magnetic configurations. The MHD-kinetic hybrid toroidal stability code MARS-K was applied to the studies, which self consistently takes into account the drift kinetic effects of thermal particles and energetic particles. Numerical analyses have been made on the results in order to provide an understanding on the mode physics. The various physics natures of the FLEM are presented and its relation with the Resistive Wall Mode (RWM) is discussed.

The FLEM in RFP plasmas is firstly presented, where the instability is predicted for non-resonant modes, which are the least stable kink modes in RFP configuration. When a sufficient fraction of EPs presents in the plasma and the condition of resonance $n\omega_{da} \approx \omega_r - n\Omega$ is satisfied, the stable non-resonant ideal kink mode (stabilized by the sufficiently closed ideal conducting wall) can be converted to a unstable FLEM by the precessional drift resonance of the EPs (hot ions). The mode frequency is linked to the precessional drift frequency of EPs and the external kink mode, therefore, is much higher than the frequency of RWMs, around the range of the ideal MHD time scale, and

varies with the plasma rotation frequency. The instability occurs at rather high plasma beta value β_p. In fact, the value of $\beta_p^{idealwall}$ is the upper-bound of the parameter region of the FLEM instability, where the external ideal kink stays near the marginal stability, thus is easiest to be excited under the ideal wall boundary. From another point of view, the energy component δW_b is small enough near $\beta_p^{idealwall}$ ($\beta_p \leq \beta_p^{idealwall}$), resulting to a sufficient low frequency ω_r of the external kink mode, which is easily match the precession frequency ω_{da} of EPs. For given parameters of EPs (ε_α, β^*), when total plasma beta value β_p decreases, δW_b increases due to decreasing of $|\delta W_F|$ (farther from the marginal state). Therefore, the external kink frequency ω_r increases with the decreasing of β_p (Eq. 21A). When ω_r becomes large enough and no longer matches the precession frequency ω_{da} of EPs to be resonance, the instability disappears. The higher fraction of EPs (with higher β^*) could provide larger contribution to δW_k^i , certainly resulting easier excitation of FLEM instability. Spatially, higher birth energy ε_α leads to higher precession frequency, which would sensitively enlarge the plasma parameter region of the unstable FLEM.

In general, the instability of FLEM does not depend on the wall resistivity. However, the wall position could significantly affect the mode property. The closer wall to the plasma, the higher plasma beta is required for the excitation of the instability. The kinetic effect of the thermal particles (transit resonance of passing particles) can cancel the driving mechanism contributed by the precession resonance of EPs, thus plays a stabilizing role on FLEMs.

With the presence of EPs in the plasma, the FLEM and the RWM can coexist. They can couple to each other if plasma rotates, depending on the plasma parameters. However, RWMs can be stabilized by the plasma rotation, while FLEMs remain unstable with the usual plasmas rotation.

The same type of the instability is observed in the Tokamak plasmas, where the (dominant) non-resonant external kink mode (e.g. m=1, n=1) couples with the resonant external kink modes (e.g. m=2, 3, n=1). The similar natures of FLEM to what mentioned above for RFPs are observed. Nevertheless, in Tokamaks the frequency of FLEM is much lower than what in RFP due to the lower precession frequency of EPs in a Tokamak than in RFP (with same birth energy). Furthermore, the Landau damping of the transit resonance by the passing thermal particles in Tokamak is weaker than in RFP due to the longer connection length in Tokamaks.

In this work, due to the non-resonant nature of the FLEMs in RFP plasmas, where the mode n=6 with most important poloidal harmonics (e.g. m=-5 to 5) are non-resonant, the Alfven continuum damping seems be rather low and does not crucially influence the instability nature. As for the tokamak, where the non-resonant harmonic (n=1, m=1) is still an important factor, although it couples with some resonant modes, we do not observe a dramatically modification on the

conclusions for the FLEM instability due to the coupling between the non-resonant and the resonant modes. This point needs to be further investigated in our future study.

Acknowledgement

This work was supported by the Euratom Communities under the contract of Association between EURATOM and ENEA, and part-funded by The RCUK Energy Programme under Grant No EP/I501045 and the European Communities under the contract of Association between EURATOM and CCFE. The views and opinions expressed herein do notnecessarily reflect those of the European Commission.